## PAPER

Check for updates

# Cerium oxide nanoparticle functionalized lignin as a nano-biosorbent for efficient phosphate removal†

Xiaohuan Liu,[ab] Xia He,[e] Jiantao Zhang,[b] Jiayao Yang,[b] Xiaofei Xiang,[c] Zhongqing Ma,[b] Lina Liu[b] and Enmin Zong [ID] *[cd]

Removing excess phosphorus is a highly effective method to prevent eutrophication in contaminated water. However, the design and preparation of an efficient biosorbent for phosphate capture is still a great challenge. We fabricated a novel, and inexpensive nano-biosorbent, L-NH$_2$@Ce, by loading cerium oxide nanoparticles (nano-CeO$_2$) within the aminated lignin using a facile *in situ* precipitation approach for efficient phosphate removal. The as-designed nano-biosorbent L-NH$_2$@Ce exhibited a BET surface area ($S_{BET}$) of 89.8 m$^2$ g$^{-1}$, 3 times that of lignin, and a pore volume ($V_p$) of 0.23 cm$^3$ g$^{-1}$. Owing to these results, the adsorption capacity of L-NH$_2$@Ce increased by 14-fold to 27.86 mg g$^{-1}$ compared with lignin (1.92 mg g$^{-1}$). Moreover, the L-NH$_2$@Ce can quickly reduce a high phosphate concentration of 10 ppm to well below the discharge standard of 0.5 ppm recommended by the World Health Organization (WHO) for drinking water. Importantly, a study of leaching tests indicated the negligible risk of Ce ion leakage during phosphate adsorption over the wide pH range of 4–9. Moreover, L-NH$_2$@Ce exhibits good reusability and retains 90% of removal efficiency after two adsorption–desorption cycles. The environmentally benignity of the raw material, the simple preparation process, and the high stability and reusability makes L-NH$_2$@Ce a promising nano-biosorbent for phosphate removal.

## 1. Introduction

Phosphorus is an essential nutrient that plays a very significant role in the growth of all living organisms.[1] Unfortunately, excess phosphorus in water bodies often causes eutrophication, leading to increase in the growth of algae, known as algal bloom, which may threaten public health and the safety of the living environment.[2] Therefore, it is important to develop efficient methods to remove excess phosphate before discharging it into water. Currently, many conventional strategies such as chemical precipitation, biological removal, electrochemical treatment, and adsorption, have been proven effective for removing phosphate from wastewater.[3] Nevertheless, these methods suffer from certain drawbacks such as high cost and

energy consumption and the requirement of a large number of chemicals, which can lead to the generation of sludge and secondary pollution.[4] Thus, it is important to explore a more effective, sustainable, and inexpensive method for removing phosphate from aqueous solutions. Previously, studies have reported bio-sorption as an attractive alternative due to its low cost and high efficiency under very low phosphate concentrations, which is beneficial for treating wastewater.[2,4–6] Hence, the development of an inexpensive and highly effective biosorbent using an abundant, sustainable, and environmentally benign material is highly required.

Lignin is the second-most abundant renewable biopolymer behind the cellulose. By one estimate, >7 × 10$^8$ tons of lignin is obtained as a waste from papermaking and biorefinery industries every year.[7–11] However, only <10% lignin is developed to be a value-added chemical and material,[12–19] and the remaining (>90%) is burned as a low-value fuel. Recently, there has been considerable interest for converting lignin into a high-performance biosorbent for removing pollutants from wastewater because of its advantages of being abundance, low cost, sustainability, environmental–friendliness, and rich reactivity.[5,18,20–22] Although a number of studies have currently examined the unitization of raw lignin as a biosorbent for capturing dyes and metal ions from wastewater, few studies have focused on exploring the ability of removing phosphate by raw lignin. Nevertheless, the phosphate adsorption capacity of

*[a]Department of Environmental Science, Zhejiang University, 388 Yuhangtong Road, Hangzhou, 310058, PR China*

*[b]Department of Materials, Zhejiang A & F University, 666 Wusu Street, Hangzhou 311300, PR China*

*[c]Department of Environmental Engineering, Taizhou University, 1139 Shifu Street, Taizhou 318000, PR China. E-mail: zongenmin@tzc.edu.cn*

*[d]School of Earth Sciences and Engineering, Nanjing University, Nanjing 210093, China*

*[e]College of Materials and Textiles, School of Art & Design, Zhejiang Sci-Tech University, Hangzhou 310018, PR China*

† Electronic supplementary information (ESI) available: The phosphate adsorption capacity of L-NH$_2$@Ce in comparison with some biosorbents. See DOI: 10.1039/c9ra09986g

raw lignin was often less because of its lack of active sites and negatively charged surfaces.[18] For example, raw lignin produced from biobutanol showed a low adsorption amount of 1.92 mg g$^{-1}$ for phosphate removal.[23] Thus, to improve the adsorption capacity of phosphate, it is very important to modify lignin.

Many studies have demonstrated that metal (hydr)oxides such as $ZrO_2$, $TiO_2$, $Fe(OH)_3$, $La(OH)_3$, and $CeO_2$ can be used to modify adsorbents for improving their specific surface areas and adsorption capacities.[24–33] $CeO_2$ is not easily soluble in acid and does not easily leak when harmful ions are removed from wastewater.[29] Thus, $CeO_2$ is considered to be one of the most attractive and promising adsorbents for capturing phosphate. For instance, both $CeO_2$-loaded nanofibers and $CeO_2$-covered $Fe_3O_4@SiO_2$ nano-adsorbents exhibited high adsorption capacity, good adsorption selectivity, and excellent stability for capturing phosphate.[30,31] However, compared with the above mentioned materials, lignin was more inexpensive and eco-friendly and could be used as a support for $CeO_2$ to improve adsorption amount of phosphate and avoid agglomeration of nano-$CeO_2$.[26] According to the best of our knowledge, the use of lignin and Ce for phosphate capture as the adsorbent is rarely reported. Thus, the effects of phosphate removal by the Ce-based adsorbents using lignin as the support would be necessary to unveil.

Herein, a novel and inexpensive lignin-based nano-cerium oxide adsorbent (L-NH$_2$@Ce) was first prepared by a facile *in situ* precipitation approach. To improve the bonding between lignin and cerium oxide, polyethylenimine (PEI) with a number of amino functional groups was grafted onto lignin to form an aminated lignin *via* the Mannich reaction (Fig. 1a), which can facilitate the loading of nano-$CeO_2$ onto the aminated lignin. Firstly, the nano-biosorbent L-NH$_2$@Ce were systematically characterized by using SEM, TEM, BET, XPS, XRD, and FTIR technologies. The adsorption performances of phosphate were then tested, including the phosphate adsorption isotherms and kinetics, the influence of pH and interfering anions on the phosphate removal efficiency as well as regeneration performance on the L-NH$_2$@Ce. Finally, the stability of Ce ions on L-NH$_2$@Ce and probable adsorption mechanism were studied. The relevant results would establish better understanding of the applicability of adsorption processes from wastewater with regard to phosphate removal by the novel nano-adsorbent L-NH$_2$@Ce.

## 2. Materials and methods

### 2.1. Materials

Lignin (catalog number 471003) was bought from Sigma-Aldrich Co., Ltd. The element compositions of lignin were 47.74 wt% C, 1.82 wt% H, 47.56 wt% O, 0.14 wt% N, and 2.74 wt% S. Cerium(III) chloride heptahydrate (catalog number C104761, 99%), poly(ethyleneimine) (catalogue number E107079, 99%), and ammonium molybdate tetrahydrate (catalog number A116375) were supplied by Aladdin Reagent Co., Ltd. Potassium antimonyl tartrate (catalog number XW2830074501), potassium dihydrogen phosphate (catalog number L01159401, $\geq$ 99.0%), sodium chloride (catalog

number 10019318, 99.5%), potassium nitrate (catalog number 10017218, 99.0%), potassium sulfate (catalog number 10017918, 99.0%), potassium hydrogen carbonate (catalog number 20030218, 99.5%), potassium hydroxide (catalog number 10017008, 85%), hydrogen chloride (catalog number 10011061, 36–38%), and formaldehyde (catalog number 10010018, 37–40%) were purchased from Sinopharm Chemical Reagent co., Ltd. Each chemical was used as-obtained.

### 2.2. Preparation of aminated lignin (L-NH$_2$)

L-NH$_2$ was prepared using a previously reported method.[15] In brief, 5.0 g lignin, 4.0 g polyethylenimine (PEI), and 4.0 g formaldehyde were added into a 250 mL three-necked flask with a solvent of 100 mL distilled water and vigorously agitated for 10 min using a magnetic stirrer. Subsequently, 1.0 M NaOH solution was slowly added into the mixture to ensure the pH value reached 10.0. Then, the above reaction mixture was maintained for 8 h at 60 °C. Finally, the resultant product was subsequently precipitated by adjusting the pH to reach 2.0–3.0 using diluted HCl. The final product was collected by suction filtration, washed repeatedly with distilled water, followed by drying in vacuum drier at 60 °C for 24 h. As shown in Fig. 1a, the brownish-black powder was denoted as L-NH$_2$ (9.295 g).

### 2.3. Preparation of cerium oxide nanoparticles functionalized aminated lignin (L-NH$_2$@Ce)

L-NH$_2$@Ce was fabricated using a facile *in situ* precipitation approach. Briefly, 2.0 g L-NH$_2$ was added in the 100 mL of deionized water containing 3.726 g of CeCl$_3$·7H$_2$O and stirred for 2 h for absorbing Ce$^{3+}$ onto the L-NH$_2$ surface. Afterwards, a certain volume of NaOH solution was slowly added into the above mixture and mixed well until the pH value changed to 10.0. After that, the resulting mixture was then conducted at 60 °C in a water bath for 2 h and later reacted at 25 °C for 24 h. Finally, the resulting product was obtained under vacuum filtration and washed repeatedly with distilled water, followed by drying in vacuum drier at 60 °C for 24 h. The obtained grayish-yellow powder was designated as L-NH$_2$@Ce (3.45 g), as shown in Fig. 1a. For comparison purpose, the pure CeO$_2$ was also prepared in the same manner as that of L-NH$_2$@Ce.

### 2.4. Adsorption experiments

The stock phosphate solution of a concentration of 1000 mg L$^{-1}$ (computed in P) was obtained by dissolving 4.3940 g anhydrous KH$_2$PO$_4$ into 1.0 L deionized water, and different required concentrations of phosphate solutions were prepared by further diluted with deionized water. To assess the phosphate adsorption behaviors of our nano-biosorbent L-NH$_2$@Ce, a series of batch adsorption experiments has been performed. The batch experiment was conducted in the 40 mL glass vials closed with PTFE-lined screw caps. At the end of adsorption performance test, the solution was first filtered through 0.45 μm membrane filter, and then the residual concentration of phosphate was determined by molybdenum blue using a T6 UV-Vis spectrophotometer. Batch experiments for phosphate adsorption were conducted in duplicate and the average values were obtained.
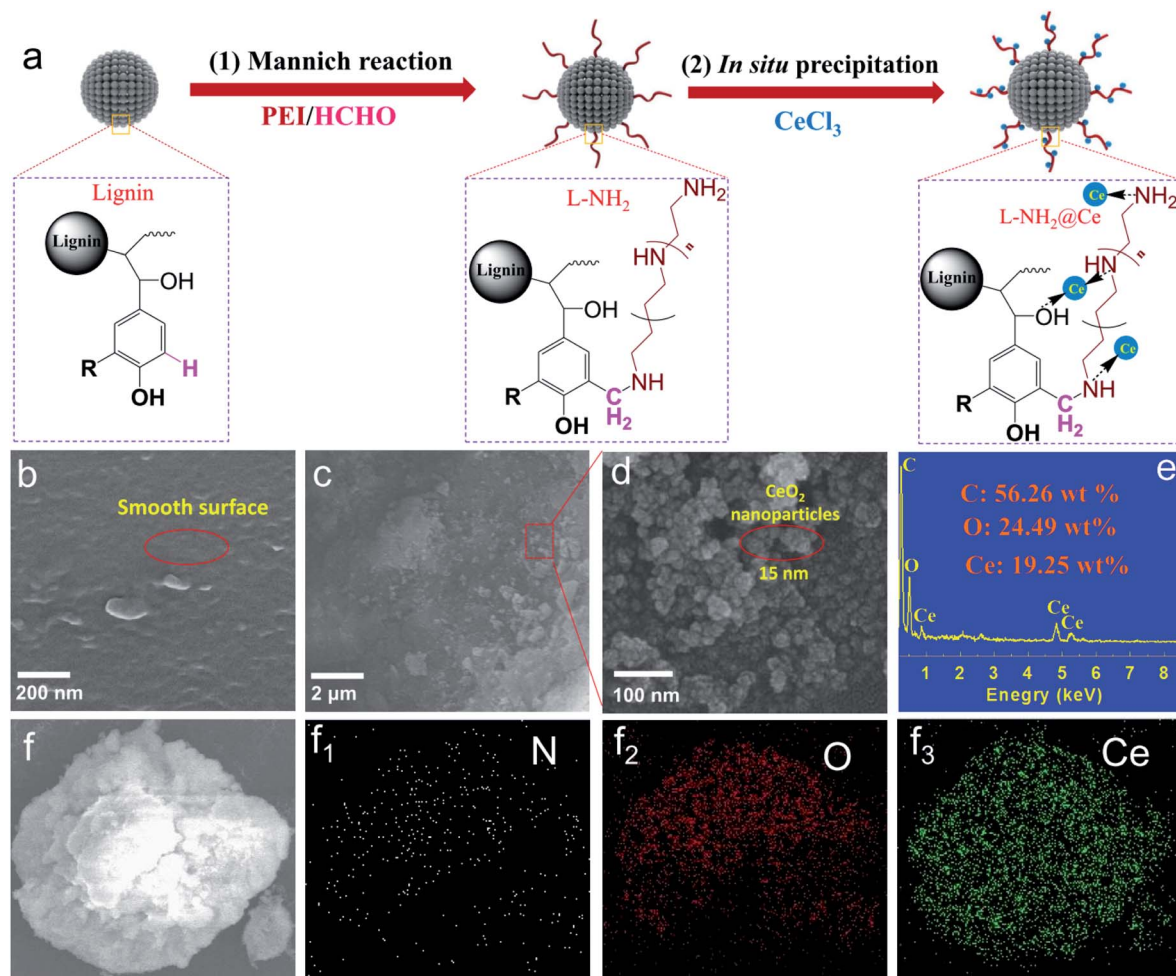
**Fig. 1** (a) Schematic for the facile preparation of biosorbent L-NH$_2$@Ce nanohybrid, and SEM micrograph for (b) L-NH$_2$, (c and d) L-NH$_2$@Ce, and (e) EDX analysis of L-NH$_2$@Ce, and (f) SEM images L-NH$_2$@Ce and (f$_1$–f$_3$) its element mapping of the corresponding N, O, and Ce.

All bath adsorption tests were carried out at 298 K with a pH 6.0 ± 0.2, except pH and temperature effects studies. The uptake amount of phosphate at equilibrium, $Q_e$ (mg g$^{-1}$), was measured using eqn (1):

$$Q_e = (C_0 - C_e)V/m \qquad (1)$$

where $C_0$ (mg L$^{-1}$) corresponds to the initial concentration of phosphate, $C_e$ (mg L$^{-1}$) refers to the equilibrium concentration of phosphate in the adsorption experiment, $V$ (mL) is total volume of the adsorption solution, and $m$ (g) is the dry weight of the adsorbent L-NH$_2$@Ce.

The removal efficiency of phosphate was determined by eqn (2):

$$R(\%) = \frac{C_0 - C_e}{C_0} \times 100\% \qquad (2)$$

**2.4.1. Adsorption isotherm.** Adsorption isotherm experiments for L-NH$_2$@Ce was conducted by adding 50 mg adsorbent into 40 mL phosphate solution with various initial phosphate concentrations in the range of 1.94–43.66 mg L$^{-1}$.

Then, each solution was agitated with an orbital shaker at room temperature at a rate of 200 rpm for 48 h to ensure that equilibrium was reached.

**2.4.2. Adsorption kinetics.** Adsorption kinetics experiments for L-NH$_2$@Ce were performed with 10 mg L$^{-1}$ phosphate concentration in a 500 mL flask with magnetic stirring. The 400 mL phosphate solution containing 0.2 g L-NH$_2$@Ce was vigorously agitated in an orbital shaker at 25 °C, and then ~1.5 mL of solution samples was withdrawn from the flask at various set time intervals from 0.5 to 600 min.

**2.4.3. Influence of pH.** To investigate the effect of pH on the adsorption performance of phosphate, six 50 mg samples of L-NH$_2$@Ce were immersed in 20 mg L$^{-1}$ phosphate solutions at initial solution pH range of 4.0 to 9.0, and then agitated on an orbital shaker set at 200 rpm at 25 °C. For adjusting the solution pH values of phosphate adsorption experiments, 0.1 M of both HCl and NaOH solutions were utilized. The leakage concentrations of Ce ions in the solutions after phosphate adsorption under different pH were obtained from Inductively Coupled Plasma-Mass Spectrometry (ICP-MS, Thermo Fisher Scientific Inc.).

**2.4.4. Influence of temperature.** To evaluate the effect of temperature on the adsorption performance of phosphate, three 50 mg samples of L-NH$_2$@Ce were immersed into 40 mL of phosphate solution at varies solution temperatures (15 °C, 25 °C, 35 °C, and 45 °C) and stirred on an orbital shaker for 24 h.

**2.4.5. Influence of coexisting anions.** To examine the effect of interfering anions on the phosphate removal performance, three types of interfering anions ($SO_4^{2-}$, $HCO_3^-$, and $NO_3^-$) with initial phosphate concentration of 100 mg L$^{-1}$ were agitated on an orbital shaker set at 200 rpm for 24 h at 25 °C.

**2.4.6. Regeneration study.** The two cycles of adsorption–desorption experiments for L-NH$_2$@Ce were investigated. The spent L-NH$_2$@Ce was regenerated by using 0.1 M NaOH solution at 60 °C for 3 h. The regenerated L-NH$_2$@Ce was collected by filtration, washed many times with distilled water, followed by drying in vacuum drier at 60 °C for 24 h, and used in the next adsorption test.

## 2.5. Characterization

**2.5.1. XPS analysis.** XPS spectra of lignin, L-NH$_2$@Ce, and L-NH$_2$@Ce after phosphate adsorption were conducted on a PHI 5000 Versa Probe with using Al Kα as the radiation source. For calibrating the binding energy value, the C 1s peak at 284.6 eV was used.

**2.5.2. FTIR analysis.** Fourier transform infrared (FTIR) spectra of lignin, L-NH$_2$@Ce, and L-NH$_2$@Ce after phosphate adsorption were collected in the range of 4000–400 cm$^{-1}$ on a Model PerkinElmer 1100 series operated using the KBr pellet technique.

**2.5.3. XRD analysis.** X-ray diffraction (XRD) spectra of the lignin and L-NH$_2$@Ce were carried out on a Rigaku D/max-RA power diffractometer with using Cu Kα the radiation source ($\lambda$ = 1.542512 Å) over the 2$\theta$ range from 10° to 80° with a scanning rate of 5° min$^{-1}$. Based on XRD data, the average crystallite diameter of L-NH$_2$@Ce was determined by the Scherrer formula: $D = K\lambda/\beta \cos \theta$, where $D$ is the crystallite diameter (nm), $\beta$ is the line-width at half maximum of the diffraction peak position (FWHM), $K$ is a dimensional shape factor, which is equal to 0.9, $\lambda$ is the average wavelength of X-ray radiation (Å), and $\theta$ is the diffracting angle (radian).

**2.5.4. SEM and EDX measurement.** Scanning electron microscopy (SEM) images and elemental data of L-NH$_2$ and L-NH$_2$@Ce were assessed using a Hitachi S-4800 field emission microscope attached to an energy-dispersive energy spectrometer (EDX). The images were collected at an accelerating voltage of 15 000 V. Prior to observation, samples were sprayed with a thin layer of gold by a sputter coater. The mean values of C, O, and Ce content (wt%) were determined from EDX by averaging three portions of the sample.

**2.5.5. TEM examination.** The structure and surface morphologies of L-NH$_2$@Ce were recorded on a JEOL JEM-1230 transmission electron microscopy (TEM) apparatus.

**2.5.6. N$_2$ adsorption–desorption analysis.** The nitrogen adsorption–desorption isotherms of L-NH$_2$ and L-NH$_2$@Ce were obtained at 77 K using a QuantachromeAutosrob-1 instrument. Before testing, the samples were treated by drying for 12 h at 105 °C. The specific surface area of lignin and L-NH$_2$@Ce were calculated by the Brunauer–Emmett–Teller (BET) model, and the average pore size and pore volume were estimated by the adsorption branch of the isotherm using the Barrett–Joyner–Halenda (BJH) model, respectively.

## 3. Results and discussion

### 3.1. Fabrication and characterization of nano-biosorbent (L-NH$_2$@Ce)

Fig. 1a shows the facile fabrication process of nano-biosorbent (L-NH$_2$@Ce). First, aminated lignin (L-NH$_2$) was obtained by Mannich reaction;[15] moreover, a number of positively charged groups (e.g., –NH– and –NH$_2$) were formed in the framework of L-NH$_2$. After CeCl$_3$ was added to the above suspension of L-NH$_2$, Ce$^{3+}$ ions attached to the L-NH$_2$ surface through coordination, and then CeO$_2$ nanoparticles were *in situ* deposited on the L-NH$_2$ surface *via* the hydrolysis of Ce$^{3+}$ ions. On filtration, CeO$_2$ nanoparticles-decorated L-NH$_2$ assembled into the target product nano-biosorbent (L-NH$_2$@Ce). The nanostructure of the L-NH$_2$@Ce was verified by SEM images (Fig. 1b–d). Compared with the smooth surface of L-NH$_2$, the L-NH$_2$@Ce clearly exhibited a typical nano-crystallite structure (average diameter = 15 nm) formed on its surface, which facilitated the creation of a porous nanostructure. Meanwhile, as shown in Fig. 1e, 56.26 wt% C, 24.49 wt% O, and 19.25 wt% Ce are observed by EDX in L-NH$_2$@Ce. The formation of nanostructure created by CeO$_2$ nanoparticles resulted in an elevation in both $S_{BET}$ and $V_P$. As shown in Fig. 2a, b and Table 1, the $S_{BET}$ of L-NH$_2$@Ce increased by two-fold to 89.8 m$^2$ g$^{-1}$ and its $V_P$ showed a four-fold increase to 0.23 cm$^3$ g$^{-1}$ compared with that of lignin. The average pore size (15.28 nm) of L-NH$_2$@Ce indicated the coexistence of mesopores. The increased $S_{BET}$ and $V_P$ of L-NH$_2$@Ce allowed the homogeneous distribution of CeO$_2$ nanoparticles, which was confirmed by EDX map scanning (Fig. 1f and f$_1$–f$_3$) and was beneficial for phosphate removal from aqueous solutions.

To confirm that CeO$_2$ was formed when Ce$^{3+}$ attached on the surface of L-NH$_2$, we utilized BET, XPS, XRD, and FTIR technologies. The XPS investigation was performed to analyze elemental composition of L-NH$_2$@Ce, which provides powerful evidence of the preparation procedure for L-NH$_2$@Ce, especially the attachment of Ce ions. The results are shown in Fig. 2c for both lignin and L-NH$_2$@Ce, containing both C and O. As for the L-NH$_2$@Ce spectrum, N can be seen, indicating that PEI was successfully introduced onto lignin based on Mannich reaction. Importantly, Ce appeared in the spectrum of L-NH$_2$@Ce because of the loaded Ce on the L-NH$_2$ surface. Moreover, as shown in Fig. 2d, the Ce 3d for L-NH$_2$@Ce was decomposed into eight characteristic peaks including 882.3 eV/900.8 eV, 884.5 eV/902.9 eV, 888.7 eV/907.4 eV and 898.3 eV/916.6 eV. The peaks at 882.3 eV/900.8 eV, 888.7 eV/907.4 eV and 898.3 eV/916.6 eV are ascribed to chemical states of Ce$^{4+}$, and the peaks at 884.5 eV/902.9 eV are due to Ce$^{3+}$. According to the fitted results, it is confirmed there are a mixed valence state of Ce$^{4+}$ and Ce$^{3+}$ on the surface of L-NH$_2$@Ce, and the ratio of Ce$^{4+}$/Ce$^{3+}$ was 7 : 3. All these XPS changes confirmed that nano-cerium oxide was
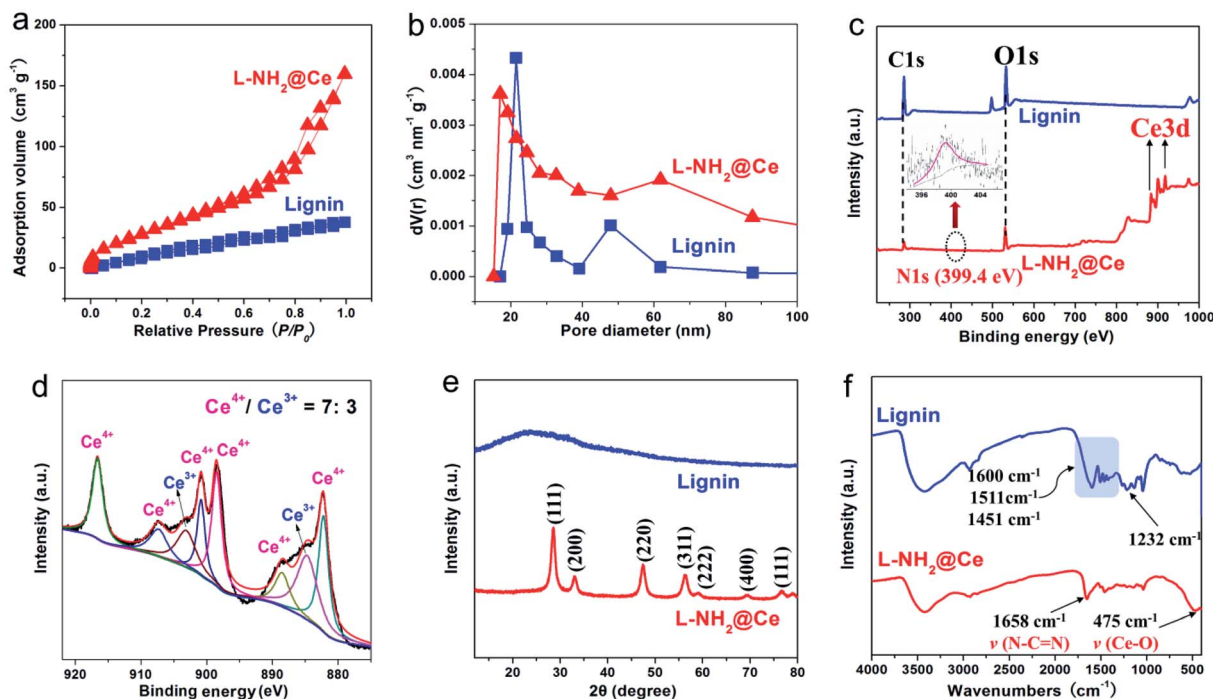
**Fig. 2** (a) Nitrogen adsorption/desorption isotherms, (b) pore size distributions, and (c) XPS spectra of lignin and L-NH₂@Ce, and (d) XPS spectra of Ce 3d for L-NH₂@Ce, and (e) XRD patterns, and (f) FTIR spectra of lignin and L-NH₂@Ce.

**Table 1** General characteristic of lignin and L-NH₂@Ce

|  | $S_{BET}$ (m² g⁻¹) | $V_P$ (cm³ g⁻¹) | $d_p$ (nm) |
|---|---|---|---|
| Lignin | 29.13 | 0.049 | 21.52 |
| L-NH₂@Ce | 89.8 | 0.23 | 15.28 |

successfully loaded on L-NH₂. XRD spectra provided robust evidence to support CeO₂ created on the surface of L-NH₂. For the XRD spectrum of lignin (Fig. 2e), a weak peak located at $2\theta = \sim 24.2°$ was observed, suggesting that lignin was largely amorphous structure in nature.[32] After lignin was functionalized, the XRD characteristic peaks were located at $2\theta$ values of 28.5° (111), 33.0° (200), 47.4° (220), and 56.2° (311), which was in consistent with the standard pattern of cubic CeO₂ (JCPDS card no. 34-0394).[29] The crystallite size of these CeO₂ nanoparticles obtained from the XRD diffraction pattern is 13 nm, calculated by the Scherrer equation, which is almost in close agreement with the aforementioned SEM result showing the average size of 15 nm. Based on these results, we can deduce that nano-CeO₂ formed when Ce³⁺ attached to the surface of L-NH₂. This indicated the successfully formation of the nano-biosorbent L-NH₂@Ce. FTIR spectra further confirmed the introduction of CeO₂, as shown in Fig. 2f. L-NH₂@Ce showed additional FT-IR characteristic peaks at 1658 cm⁻¹ and 475 cm⁻¹ compared with lignin, which can be related to the N–C=N and Ce–O stretching vibrations, respectively.[30] Thus, we conclude that the nano-biosorbent L-NH₂@Ce was successfully prepared.

## 3.2. Adsorption kinetic

Adsorption kinetic experiment was conducted to evaluate the adsorption rate of phosphate, and the relevant results are presented in Fig. 3a. Note that >80% of the phosphate was removed just after 1 min. After ∼60 min of exposure, we reached adsorption saturation, and 97% of the phosphate ions were removed by L-NH₂@Ce. Such a quick removal rate for as-obtained L-NH₂@Ce exhibits the attractive and promising potential towards practical application in treating real life and industrial wastewater containing phosphate. Moreover, the adsorption rate of L-NH₂@Ce was higher than that of some materials for phosphate adsorption.[23,35] More importantly, the residue concentration of phosphate on L-NH₂@Ce decreased to 0.1 ppm, far below phosphate discharge recommended by WHO for drinking water,[36] further illustrating that the L-NH₂@Ce could be effectively and quickly for eliminating phosphate from wastewater. To acquire more information regarding the adsorption behavior, the experimental kinetic data were fitted by using the following linear formulas, such as the pseudo-first-order model (eqn (3)), and pseudo-second-order model (eqn (4)).[35,37,38]

$$\log(Q_e - Q_t) = \log Q_e - \frac{k_1 t}{2.303} \quad (3)$$

$$\frac{t}{Q_t} = \frac{1}{k_2 Q_e^2} + \frac{t}{Q_e} \quad (4)$$

where $Q_t$ (mg g⁻¹) is the uptake amount of phosphate at a certain time $t$; $Q_e$ (mg g⁻¹) is the uptake amount of phosphate at equilibrium; $t$ (min) is the contact time; $k_1$ (min⁻¹) is the
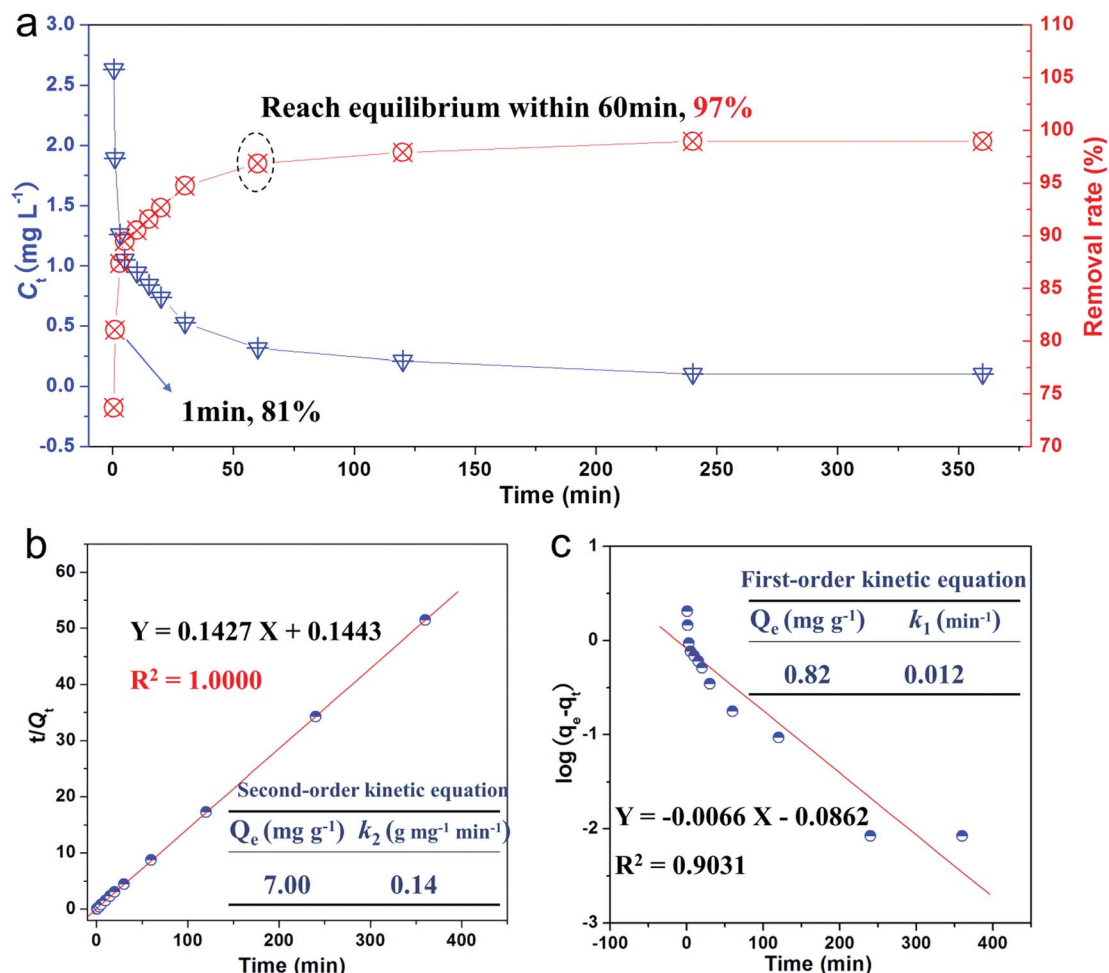
Fig. 3 (a) Adsorption kinetics of phosphate on L-NH$_2$@Ce, and fitting results for (b) pseudo-second-order model and (c) pseudo-first-order model on L-NH$_2$@Ce.

adsorption rate constant for the first order model; and $k_2$ (g mg$^{-1}$ min$^{-1}$) is the adsorption rate constant for the second order model. According to the derived kinetic parameters for eqn (3) and (4) (Fig. 3b and c), note that the adsorption of phosphate on the L-NH$_2$@Ce complied well with the pseudo-second order model due to a high correlation coefficient of 1.0000. Additionally, the equilibrium adsorption amounts (7.00 mg g$^{-1}$) calculated from fitting result is good agreement with the experimental data (6.99 mg g$^{-1}$), confirming that the kinetic of phosphate adsorption to L-NH$_2$@Ce follows the pseudo-second order model, indicating a chemisorption process.[5]

The structures of Ce component in the functionalized composites after adsorption were investigated by FTIR (Fig. 4a). The primary characteristic peaks remained after phosphate adsorption, suggesting the structural integrity of the as-obtained L-NH$_2$@Ce. Moreover, a sharp band was observed at 475 cm$^{-1}$, which is attributed to the binding vibrations of –OH of CeO$_2$. Moreover, two new absorption peaks at ~1035 cm$^{-1}$ (P–OH) and ~1152 cm$^{-1}$ (P=O) appeared, which strongly confirms the presence of phosphate after phosphate-adsorbed

L-NH$_2$@Ce and indicates the reliable complexation between Ce–OH functional groups of L-NH$_2$@Ce and phosphate through the Ce–O–P coordination bonds.[36] Meanwhile, XPS spectra provide additional evidence for the adsorption of phosphate on L-NH$_2$@Ce. Compared to the original L-NH$_2$@Ce, the appearance of P 2p peak after phosphate adsorption confirms the successful attachment of phosphate onto L-NH$_2$@Ce (Fig. 4b). Note that phosphate-adsorbed L-NH$_2$@Ce showed a negative shift of ~0.7 eV compared to the purified NaH$_2$PO$_4$ (ca. 133.9 eV),[2] which is indicative of strong coordination bonds between phosphate and L-NH$_2$@Ce and contributes to the formation of CePO$_4$.[30] Furthermore, in good agreement with the FT-IR results, after the phosphate adsorption, the high resolution scan of O 1s spectra in Fig. 4c is deconvoluted into four peaks,[39] which are attributed to O in P–O (529.5 eV), H$_2$O (530.9 eV), Ce–OH (532.3 eV), and Ce–O (533.2 eV), respectively, thus verifying the strong affinity of Ce–OH toward phosphate through a complexation reaction. The SEM image of phosphate-adsorbed L-NH$_2$@Ce shows the formation of some nanoscale CePO$_4$ crystals (Fig. 4d). Moreover, the SEM-EDX measurements (Fig. 4e) confirm the presence of C, O, Ce, and P. The emergence
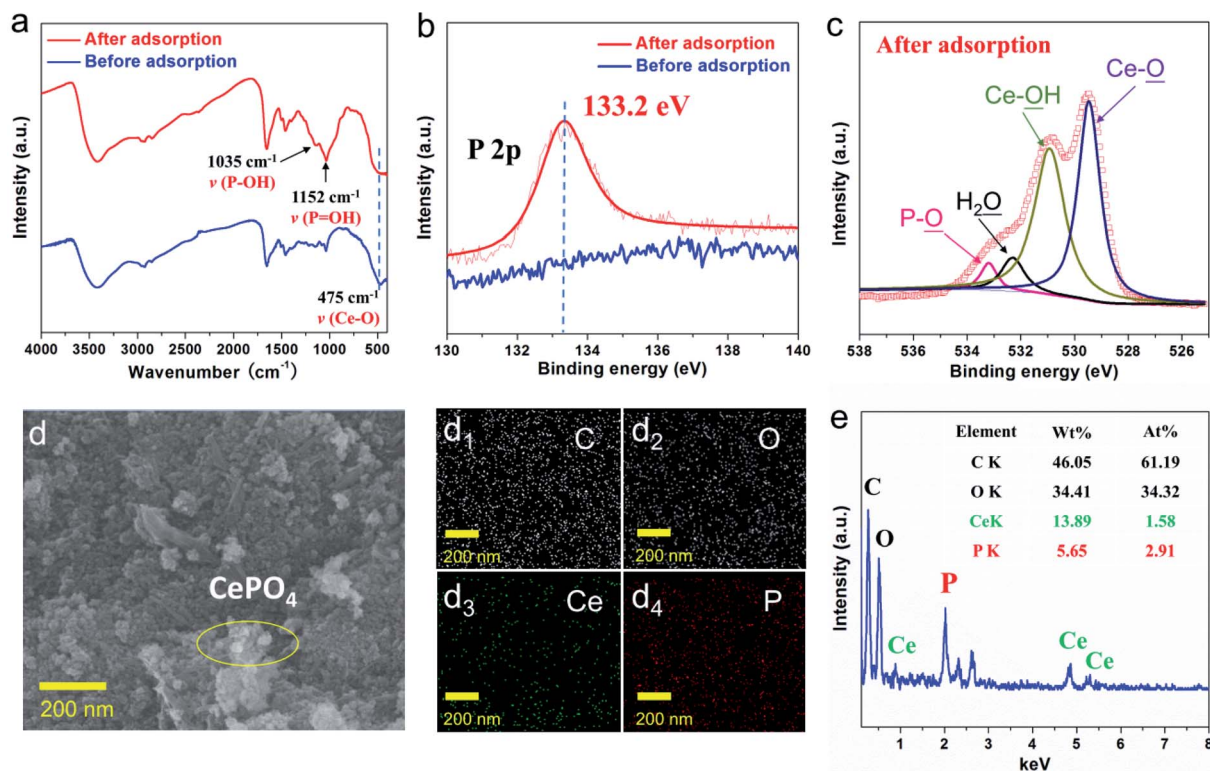
Fig. 4 (a) FTIR spectra and (b) XPS$_{P\ 2p}$ spectra of L-NH$_2$@Ce before and after phosphate adsorption. (c) XPS$_{O\ 1s}$ spectra and (d) SEM image and its element mapping of the corresponding C (d$_1$), O (d$_2$), Ce (d$_3$) and P (d$_4$) and (e) EDX spectrum of L-NH$_2$@Ce after adsorption phosphate.

of phosphorus (5.65 wt%) further validated the occurrence of phosphate attached onto the L-NH$_2$@Ce. Furthermore, EDX map scanning (Fig. 4d$_1$–d$_4$) of phosphate-attached L-NH$_2$@Ce indicates that the P element is evenly dispersed over the sample, verifying that the adsorption occurs in the whole framework of L-NH$_2$@Ce. Therefore, the formation of insoluble CePO$_4$ contributes to the phosphate removal.[40]

### 3.3. Adsorption isotherm

To determine the uptake amount of phosphate on L-NH$_2$@Ce, we obtained adsorption isotherm for a series of different initial phosphate concentrations in the range of 1.94–43.66 mg L$^{-1}$ at 25 °C (Fig. 5a). When the initial phosphate concentration increased, the uptake amount of phosphate significantly increased and then reached an equilibrium. Moreover, the effect of initial phosphate concentrations on the removal efficiency was also investigated (Fig. 5b). Over 90% adsorption efficiency of phosphate was removed below the concentration of 17.7 mg L$^{-1}$, indicative of the high efficiency for phosphate removal on L-NH$_2$@Ce. In this study, Freundlich (eqn (5)), Langmuir (eqn (6)), and Temkin models (eqn (7)) were selected to fit our experimental data.[18,20,41–44]

$$\ln Q_e = \ln K_F + \frac{1}{n} \ln C_e \tag{5}$$

$$\frac{1}{Q_e} = \frac{1}{Q_m b C_e} + \frac{1}{Q_m} \tag{6}$$

$$Q_e = A + B \ln C_e \tag{7}$$

where $Q_e$ (mg g$^{-1}$) represents adsorption amount at equilibrium; $C_e$ represents the phosphate concentration at equilibrium (mg L$^{-1}$); $Q_m$ (mg g$^{-1}$) refers to the maximum adsorption capacity of phosphate; $K_F$ and $n$ refer to the constants of Freundlich; $b$ (L mg$^{-1}$) represents the constant of Langmuir model; and $A$ and $B$ refer to the constants of Temkin model.

As shown in Fig. 5c, the adsorption isotherm is found to comply well the Langmuir model and exhibits a higher $R^2$ of 0.9933 compared with that fitted by using the Freundlich model ($R^2 = 0.9180$) (Fig. 5d) and Temkin model ($R^2 = 0.9876$) (Fig. 5e), indicating a chemical heterogeneity of the adsorbent.[5] Note that the adsorption capacity of phosphate by L-NH$_2$@Ce was calculated to be 27.86 mg g$^{-1}$ by Langmuir model (Fig. 5c and f), while that of lignin without loading CeO$_2$ showed a poor phosphate adsorption performance of 1.92 mg g$^{-1}$.[23] Meanwhile, aminated lignin (L-NH$_2$) shows a phosphate adsorption capability of 14.90 mg g$^{-1}$, which is because of the electrostatic interactions between amino groups and phosphate ions (Fig. 5g). Thus, adsorption capability of L-NH$_2$@Ce was over 14 times than that of lignin, and around 2 times that of L-NH$_2$, indicating that the functionalization of CeO$_2$ was a feasible strategy for improving phosphate capture ability of lignin. Moreover, given 19.25 wt% Ce in the L-NH$_2$@Ce, the Ce content-normalized adsorption capacity is calculated to be 145 mg g$^{-1}$ (Ce), which is much higher than that of pure CeO$_2$ (21 mg g$^{-1}$
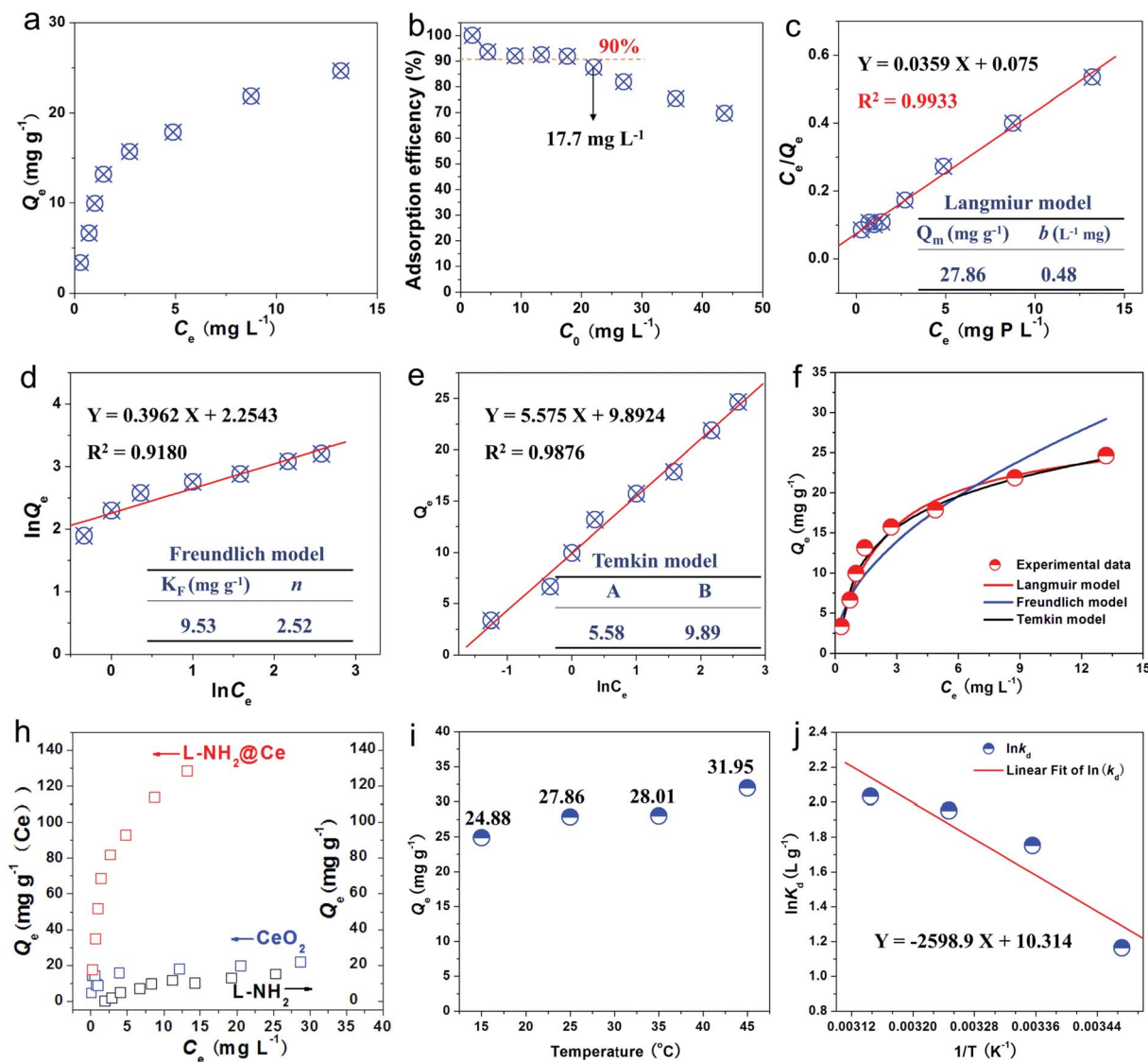
Fig. 5 (a) Phosphate adsorption isotherms, (b) effect of the initial concentration of phosphate on the adsorption efficiency for L-NH$_2$@Ce, and linear fitting results for (c) Langmuir model, (d) Freundlich model, and (e) Temkin model on L-NH$_2$@Ce, and (f) nonlinear fitting for phosphate adsorption isotherms, (g) Ce content normalized phosphate adsorption isotherms of L-NH$_2$@Ce and pure CeO$_2$, and phosphate adsorption isotherms of L-NH$_2$, (h) effect of the temperature on the uptake amount of phosphate on L-NH$_2$@Ce, and (i) plot of ln $k_d$ vs. 1/$T$ for phosphate removal by L-NH$_2$@Ce.

(Ce)) (see Fig. 5g). This is mainly because that well-dispersed CeO$_2$ nanoparticles in the L-NH$_2$ that provides more CeO$_2$ active sites exposed for phosphate adsorption. Furthermore, certain materials have been used for removing phosphate,[1,18,23,33–35,45–49] as summarized in Table S1.† As-fabricated L-NH$_2$@Ce exhibited a high adsorption capacity of phosphate than some of the previously reported biosorbents, such as Ce/Fe$_3$O$_4$-BC (18.75 mg g$^{-1}$), Fe-CL (0.942 mg g$^{-1}$), LBR-Zr (8.75 mg g$^{-1}$), ILO (4.785 mg g$^{-1}$), iron hydroxide eggshell (14.49 mg g$^{-1}$). However, the adsorption capacity of L-NH$_2$@Ce was not high compared with some reported biosorbent such as Ws-N-Zr (31.9 mg g$^{-1}$). Ws-N-Zr performed about 1.2 times phosphate adsorption capacity of L-NH$_2$@Ce. Nevertheless, Ws-N-Zr adsorption result was achieved with a long equilibrium time of 120 min under the same initial concentration of around

10 mg L$^{-1}$. Although the phosphate adsorption capacity of as-fabricated nano-biosorbent L-NH$_2$@Ce was not very significant, the lignin was still the recommended raw material to developing biosorbent for removing phosphate due to its merits of being abundant, low-cost, sustainable and environmentally benign material. Based on above results and analysis, it is promising for the utilization of L-NH$_2$@Ce in the remediation of phosphate from wastewater.

### 3.4. Effect of temperature

Fig. 5h presents the effect of temperature on the phosphate-uptake by L-NH$_2$@Ce. With the temperature increasing from 15 to 45 °C, the uptake amount of phosphate increased from 24.88 to 31.95 mg g$^{-1}$, indicative of more efficient for phosphate

**Table 2** The thermodynamic parameters for adsorption of phosphate onto L-NH$_2$@Ce

| Temperatures (K) | Thermodynamic parameters | | |
|---|---|---|---|
| | $\Delta G^0$ (kJ mol$^{-1}$) | $\Delta H^0$ (kJ mol$^{-1}$) | $\Delta S^0$ (J mol$^{-1}$ K$^{-1}$) |
| 288 | −3.089 | 21.607 | 52 |
| 298 | −3.947 | 21.607 | 52 |
| 308 | −4.804 | 21.607 | 52 |
| 318 | −5.662 | 21.607 | 52 |

adsorption at a high temperature. The possible reason for this phenomenon is that the mobility of phosphate molecules increased at a high temperature, thereby increasing collision frequency between L-NH$_2$@Ce and phosphate and improving the adsorption capacity of phosphate.[42] Furthermore, the adsorption thermodynamics of phosphate were studied. The related parameters, *i.e.*, standard free energy change ($\Delta G^0$), standard enthalpy change ($\Delta H^0$), and standard entropy change ($\Delta S^0$), can be calculated using the following formulas ((8)–(10)).[41,45]

$$\Delta G^0 = -RT \ln k_d \tag{8}$$

$$\Delta G^0 = \Delta H^0 - T\Delta S^0 \tag{9}$$

$$\ln k_d = \frac{\Delta S^0}{R} - \frac{\Delta H^0}{RT} \tag{10}$$

Based on the van't Hoff formula, the equilibrium constant $k_d$ is calculated from the slope of the plot $\ln (Q_e/C_e)$ *versus* $C_e$ at 288, 298, 308 and 318 K and extrapolating $C_e$ to zero. Note that both $\Delta H^0$ and $\Delta S^0$ values were obtained from the slope and intercept of a plot of $\ln k_d$ *vs.* $1/T$ (Fig. 5i). Moreover, the values of related parameters are summarized in Table 2. The value of $\Delta G^0$ becomes more negative with temperature increases, indicative of the spontaneous nature of phosphate adsorption
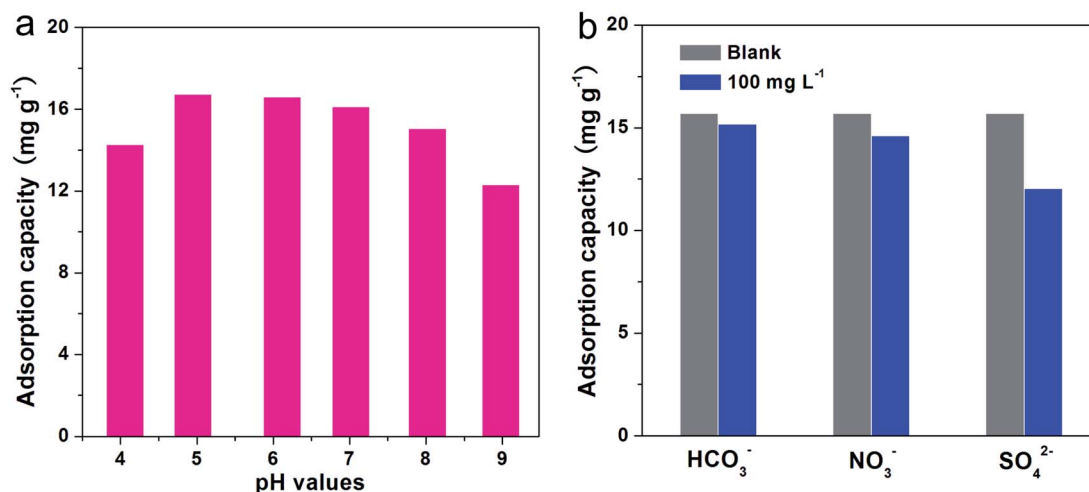
on L-NH$_2$@Ce. Note that the value of $\Delta H^0$ is positive of 21.607 kJ mol$^{-1}$, which indicates that this adsorption reaction was endothermic in nature. Similarly, the value of $\Delta S^0$ is positive of 52 J mol$^{-1}$ K$^{-1}$, which suggests an increase in the randomness of the solid/solution system and helps in the adsorption of phosphate on L-NH$_2$@Ce.[35]

### 3.5. Effect of pH values

pH value is an extremely important influence on the surface charges of sorbent and existence of phosphate species in aqueous solutions.[47,48] Thus, we examined the effect of pH value on the uptake amount of phosphate for L-NH$_2$@Ce, which is presented in Fig. 6a. The adsorption amount of phosphate increased from pH 4 to 5, and then dropped from pH 5 to 9. The highest phosphate adsorption amount of 16.73 mg g$^{-1}$ was obtained at pH 5, and the adsorption amount of phosphate considerably declined when the pH value increased to 9. This phenomenon was possibly observed because the competitive relationship between the negative OH$^-$ and PO$_4^{3-}$ for the active sites of the L-NH$_2$@Ce becomes stronger,[50] resulting in the lower adsorption amount of phosphate at high pH values such as 9. Note that similar adsorption behaviors have been observed by some adsorbents.[30,51] Based on these results, as-obtained biosorbent L-NH$_2$@Ce can effectively capture PO$_4^{3-}$ under mildly acidic, neutral, and mildly alkali conditions within the pH values range of 5–8.

### 3.6. Effect of interfering anions

In water sources, conventional anions such as HCO$_3^-$, NO$_3^-$, and SO$_4^{2-}$ usually coexist and compete with PO$_4^{3-}$ for the active adsorption sites on L-NH$_2$@Ce. Therefore, we examined the effect of interfering anions on the uptake amount of phosphate, which is shown in Fig. 6b. Interference tests were conducted by observing the changes of phosphate-uptake amount in the presence of the coexisting anion concentration at 100 mg L$^{-1}$; the initial concentration of phosphate was ~20 mg L$^{-1}$. Note that the concentration of interfering ion was four times higher



**Fig. 6** (a) Effect of solution pH values and (b) coexisting anions on the uptake amount of phosphate for L-NH$_2$@Ce.
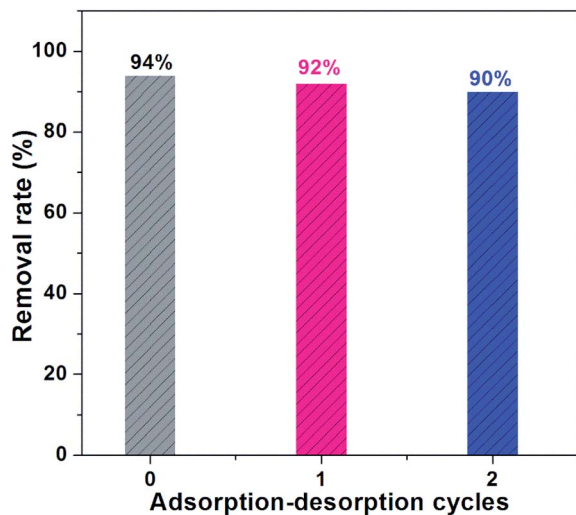
**Fig. 7** Cycle adsorption and regeneration of L-NH$_2$@Ce.

than that of phosphate. The introduction of interferents (HCO$_3^-$ and NO$_3^-$) did not generate any great alteration in the adsorption capacity for phosphate, indicating an excellent anti-interference ability of L-NH$_2$@Ce over two coexisting anions. However, the existence of SO$_4^{2-}$ caused a remarkable reduction in the phosphate adsorption amount from 15.7 mg g$^{-1}$ to 12.0 mg g$^{-1}$ because, similar to Ce$^{4+}$, SO$_4^{2-}$ could associate with the functional group on the surface of L-NH$_2$@Ce and generate strong surface complexes and decreased surface potential.[52] Therefore, the available adsorption active sites of L-NH$_2$@Ce reduced, which restrained the capture ability of phosphate. With these results, the effect of SO$_4^{2-}$ on adsorption performance was stronger than that of HCO$_3^-$ and NO$_3^-$.

### 3.7. Regeneration study

The reusability performance of the adsorbent is very significant for its practical engineering application.[53,54] Therefore,



**Fig. 8** The released Ce concentrations and calculated mass percentages of Ce leaching during phosphate adsorption at different pH values.

adsorption–desorption cycles of bath experiments were performed to investigate the reusability performance of L-NH$_2$@Ce for phosphate removal (Fig. 7). After adsorption, the used absorbent was regenerated by using 0.1 M NaOH solution at 60 °C for two times to remove the adsorbed phosphate. It can be seen that the regenerated L-NH$_2$@Ce reached 92% of phosphate removal efficiency for the first regeneration. For the second regeneration, the removal efficiency of phosphate is still high and remained at ∼90%. The slight decrease from 94% to 90% is probably because of the inevitable loss of the active sites after two regeneration cycles.[25]

### 3.8. Stability of Ce ions on L-NH$_2$@Ce

The stability of L-NH$_2$@Ce was studied by detecting Ce leaching during phosphate adsorption at different pH values.[54] As shown in Fig. 8, the released concentrations of Ce ions were 0.021, 0.015, 0.028, 0.056, 0.025, and 0.062 mg L$^{-1}$ at pH 4.0, 5.0, 6.0, 7.0, 8.0, and 9.0, respectively. The calculated leaching mass percentages of Ce were only 0.0087%, 0.0062%, 0.0116%, 0.0232%, 0.0104%, and 0.0258%, respectively, each of which was lower than that of the reported material (0.79%),[55] indicating that leaching of Ce from L-NH$_2$@Ce was negligible and most of the Ce in L-NH$_2$@Ce remained after phosphate adsorption over a wide pH range of 4–9. This was mainly because of the strong interactions between the surface groups –NH$_2$/–NH– of L-NH$_2$@Ce and nano-CeO$_2$. This feature indicated the L-NH$_2$@Ce was fairly stable in wastewater treatment.

## 4. Conclusions

In this study, a novel and inexpensive nano-biosorbent L-NH$_2$@Ce was prepared by loading nano-CeO$_2$ onto the aminated lignin, which is considered to be a promising biosorbent for phosphate capture. The crystallite size of nano-CeO$_2$ obtained from the XRD diffraction pattern is 13 nm, which is almost in close agreement with the SEM result showing the average size of 15 nm. X-ray photoelectron spectroscopy (XPS) analysis indicated 70% of Ce$^{4+}$ and 30% of Ce$^{3+}$ were on the surface of L-NH$_2$@Ce. Note that as-fabricated L-NH$_2$@Ce possessed a higher BET surface area of 89.8 m$^2$ g$^{-1}$ and higher pore volume of 0.23 cm$^3$ g$^{-1}$ than that of raw material lignin. Moreover, as compared with lignin, the as-obtained L-NH$_2$@Ce exhibits enhanced adsorption capacity of phosphate. The adsorption kinetics of phosphate onto L-NH$_2$@Ce were found to be well described by the pseudo-second-order model, indicative of a chemical interaction between phosphate and L-NH$_2$@Ce. Note that the adsorption isotherm of phosphate onto L-NH$_2$@Ce can be fitted to the Langmuir model. Furthermore, coexisting anions study indicates that the introduction of SO$_4^{2-}$ has the largest influence on the adsorption performance of phosphate. Moreover, L-NH$_2$@Ce can effectively capture phosphate under mildly acidic, neutral, and mildly alkali conditions in the pH range of 5–8. Based on these results, we can confirm that this study provides a new strategy to develop an efficient nano-biosorbent for phosphate removal.
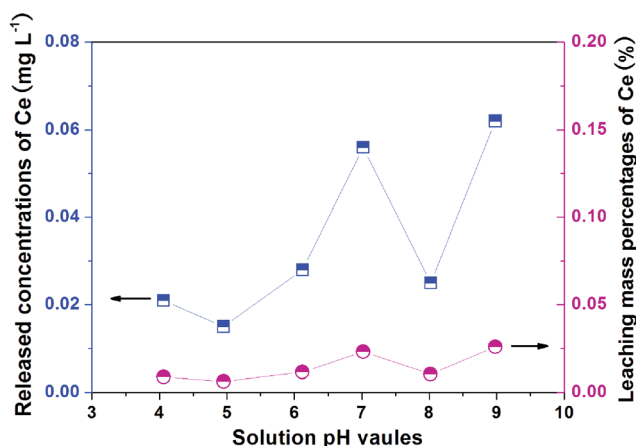
## Author contributions

Xiaohuan Liu, Xia He and Jiantao Zhang contributed equally to this work.

## Conflicts of interest

There are no conflicts to declare.

## Acknowledgements

## References

1 L. Wang, J. Wang, C. He, W. Lyu, W. Zhang, W. Yan and L. Yang, *Colloids Surf., A*, 2019, **561**, 236–243.

2 E. Zong, G. Huang, X. Liu, W. Lei, S. Jiang, Z. Ma, J. Wang and P. Song, *J. Mater. Chem. A*, 2018, **6**, 9971–9983.

3 E. Zong, X. Liu, J. Wang, S. Yang, J. Jiang and S. Fu, *J. Mater. Sci.*, 2017, **52**, 7294–7310.

4 B. Wang, J. Wen, S. Sun, H. Wang, S. Wang, Q. Liu, A. Charlton and R. Sun, *Ind. Crops Prod.*, 2017, **108**, 72–80.

5 E. Zong, D. Wei, H. Wan, S. Zheng, Z. Xu and D. Zhu, *Chem. Eng. J.*, 2013, **221**, 193–203.

6 B. Wang, J. Xia, L. Mei, L. Wang and Q. Zhang, *ACS Sustainable Chem. Eng.*, 2018, **6**, 1343–1351.

7 E. Zong, X. Liu, L. Liu, J. Wang, P. Song, Z. Ma, J. Ding and S. Fu, *ACS Sustainable Chem. Eng.*, 2018, **6**, 337–348.

8 X. Qiao, C. Zhao, Q. Shao and M. Hassan, *Energy Fuels*, 2018, **32**, 6022–6030.

9 L. Liu, M. Qian, P. Song, G. Huang, Y. Yu and S. Fu, *ACS Sustainable Chem. Eng.*, 2016, **4**, 2422–2431.

10 Y. Yu, P. Song, C. Jin, S. Fu, L. Zhao, Q. Wu and J. Ye, *Ind. Eng. Chem. Res.*, 2012, **51**, 12367–12374.

11 Y. Yu, S. Fu, P. Song, X. Luo, Y. Jin, F. Lu, Q. Wu and J. Ye, *Polym. Degrad. Stab.*, 2012, **97**, 541–546.

12 P. Song, Z. Cao, Q. Meng, S. Fu, Z. Fang and Q. Wu, *J. Macromol. Sci., Part B: Phys.*, 2012, **51**, 720.

13 P. Song, Z. Cao, S. Fu, Z. Fang, Q. Wu and J. Ye, *Thermochim. Acta*, 2011, **518**, 59–65.

14 Z. Ma, J. Wang, H. Zhou, Y. Zhang, Y. Yang, X. Liu, J. Ye, D. Chen and S. Wang, *Fuel Process. Technol.*, 2018, **181**, 142–156.

15 L. Liu, G. Huang, P. Song, Y. Yu and S. Fu, *ACS Sustainable Chem. Eng.*, 2016, **4**, 4732–4742.

16 C. Scarica, R. Suriano, M. Levi, S. Turri and G. Griffini, *ACS Sustainable Chem. Eng.*, 2018, **6**, 3392–3401.

17 X. Liu, E. Zong, W. Hu, P. Song, J. Wang, Q. Liu, Z. Ma and S. Fu, *ACS Sustainable Chem. Eng.*, 2019, 7, 758–768.

18 X. Luo, C. Liu, J. Yuan, X. Zhu and S. Liu, *ACS Sustainable Chem. Eng.*, 2017, **5**, 6539–6547.

19 X. Liu, Y. Xu, J. Yu, S. Li, J. Wang, C. Wang and F. Chu, *Int. J. Biol. Macromol.*, 2014, **67**, 483–489.

20 Z. Li, D. Xiao, Y. Ge and S. Koehler, *ACS Appl. Mater. Interfaces*, 2015, 7, 15000–15009.

21 Y. Ge and Z. Li, *ACS Sustainable Chem. Eng.*, 2018, **6**, 7181–7192.

22 V. Nair, A. Panigrahy and R. Vinu, *Chem. Eng. J.*, 2014, **254**, 491–502.

23 E. Zong, X. Liu, J. Jiang, S. Fu and F. Chu, *Appl. Surf. Sci.*, 2016, **387**, 419–430.

24 B. Wu, L. Fang, J. D. Fortner, X. Guan and I. M. C. Lo, *Water Res.*, 2017, **126**, 179–188.

25 S. Dong, Y. Wang, Y. Zhao, X. Zhou and H. Zheng, *Water Res.*, 2017, **126**, 433–441.

26 Y. Feng, H. Lu, Y. Liu, L. Xue, D. D. Dionysiou, L. Yang and B. Xing, *Chemosphere*, 2017, **185**, 816–825.

27 N. Wang, J. Feng, J. Chen, J. Wang and W. Yan, *Chem. Eng. J.*, 2017, **316**, 33–40.

28 G. Cui, M. Liu, Y. Chen, W. Zhang and J. Zhao, *Carbohydr. Polym.*, 2016, **154**, 40–47.

29 R. Li, Q. Li, S. Gao and J. K. Shang, *Chem. Eng. J.*, 2012, **185–186**, 127–135.

30 Y. Ko, T. Do, Y. Chun, C. Kim, U. Choi and J. Kim, *J. Hazard. Mater.*, 2016, **307**, 91–98.

31 J. Liu, J. Cao, Y. Hu, Y. Han and J. Zhou, *Water Sci. Technol.*, 2017, **76**, 2867–2875.

32 A. K. Kumar, B. S. Parikh and M. Pravakar, *Environ. Sci. Pollut. Res.*, 2016, **23**, 9265–9275.

33 T. Nguyen, H. Ngo, W. Guo, J. Zhang, S. Liang and K. Tung, *Bioresour. Technol.*, 2013, **150**, 42–49.

34 T. Eberhardt, S. Min and J. Han, *Bioresour. Technol.*, 2006, **97**, 2371–2376.

35 M. Rashid, N. Price, M. Gracia Pinilla and K. O'Shea, *Water Res.*, 2017, **123**, 353–360.

36 Y. Gu, D. Xie, Y. Ma, W. Qin, H. Zhang, G. Wang, Y. Zhang and H. Zhao, *ACS Appl. Mater. Interfaces*, 2017, **9**, 32151–32160.

37 H. Trivedi, V. Patel and R. Patel, *Eur. Polym. J.*, 1973, **9**, 525–531.

38 Y. Ho and G. McKay, *Process Biochem.*, 1999, **34**, 451–465.

39 Y. Yu, C. Zhang, L. Yang and J. Paul Chen, *Chem. Eng. J.*, 2017, **315**, 630–638.

40 J. He, Y. Xu, W. Wang, B. Hu, Z. Wang, X. Yang, Y. Wang and L. Yang, *Chem. Eng. J.*, 2020, **379**, 122431.

41 J. Lǚ, H. Liu, R. Liu, X. Zhao, L. Sun and J. Qu, *Powder Technol.*, 2013, **233**, 146–154.

42 S. Vasudevan and J. Lakshmi, *RSC Adv.*, 2012, **2**, 5234–5242.

43 K. Kim, D. Kim, T. Kim, B. G. Kim, D. Ko, J. Lee, Y. J. Han, J. Jung and H. Na, *RSC Adv.*, 2019, **9**, 15257–15264.

44 J. Sun, Y. Xiu, K. Huang, J. Yu, S. Alam, H. Zhu and Z. Guo, *RSC Adv.*, 2018, **8**, 22276–22285.

45 N. Mezenner and A. Bensmaili, *Chem. Eng. J.*, 2009, **147**, 87–96.

46 J. Ray, S. Jana and T. Tripathy, *Int. J. Biol. Macromol.*, 2018, **109**, 492–506.

47 B. Hui, Y. Zhang and L. Ye, *Chem. Eng. J.*, 2014, **235**, 207–214.

48 H. Qiu, C. Liang, X. Zhang, M. Chen, Y. Zhao, T. Tao, Z. Xu and G. Liu, *ACS Appl. Mater. Interfaces*, 2015, **7**, 20835–20844.

49 Y. Zhang, H. Li, Y. Zhang, F. Song, X. Cao, X. Lyu, Y. Zhang and J. Crittenden, Statistical optimization and batch studies on adsorption of phosphate using Al-eggshell, *Adsorpt. Sci. Technol.*, 2018, **36**, 999–1017.

50 H. Hao, Y. Wang and B. Shi, *Water Res.*, 2019, **155**, 1–11.

51 Y. Zhang, B. Pan, C. Shan and X. Gao, *Environ. Sci. Technol.*, 2016, **50**, 1447–1454.

52 X. Liu and L. Zhang, *Powder Technol.*, 2015, **277**, 112–119.

53 M. Kim, H. Kim and S. Byeon, *ACS Appl. Mater. Interfaces*, 2017, **9**, 40461–40470.

54 T. Li, X. Su, X. Yu, H. Song, Y. Zhu and Y. Zhang, *Bioresour. Technol.*, 2018, **263**, 207–213.

55 J. Yang, P. Yuan, H. Chen, J. Zou, Z. Yuan and C. Yu, *J. Mater. Chem.*, 2012, **22**, 9983–9990.